Published in final edited form as:
Cell Motil Cytoskeleton. 2009 January ; 66(1): 10–23. doi:10.1002/cm.20321.

Phosphorylation of Tropomyosin Extends Cooperative Binding of Myosin Beyond a Single Regulatory Unit

Vijay S. Rao, **Ellisha N. Marongelli**, and **William H. Guilford***
Department of Biomedical Engineering, University of Virginia, Charlottesville, Virginia

Abstract

Tropomyosin (Tm) is one of the major phosphoproteins comprising the thin filament of muscle. However, the specific role of Tm phosphorylation in modulating the mechanics of actomyosin interaction has not been determined. Here we show that Tm phosphorylation is necessary for long-range cooperative activation of myosin binding. We used a novel optical trapping assay to measure the isometric stall force of an ensemble of myosin molecules moving actin filaments reconstituted with either natively phosphorylated or dephosphorylated Tm. The data show that the thin filament is cooperatively activated by myosin across regulatory units when Tm is phosphorylated. When Tm is dephosphorylated, this "long-range" cooperative activation is lost and the filament behaves identically to bare actin filaments. However, these effects are not due to dissociation of dephosphorylated Tm from the reconstituted thin filament. The data suggest that end-to-end interactions of adjacent Tm molecules are strengthened when Tm is phosphorylated, and that phosphorylation is thus essential for long range cooperative activation along the thin filament.

Keywords

thin filament activation; laser trap; isometric force; in vitro motility; crossbridge kinetics

INTRODUCTION

The thin filament-associated coiled-coil dimer tropomyosin (Tm) is involved in regulating the actomyosin system by steric hindrance of myosin in the absence of calcium. However, when myosin does bind, it cooperatively activates the thin filament, allowing additional myosin to bind readily [Bremel and Weber, 1972; Greene and Eisenberg, 1980; Hill et al., 1980]. This can be modeled as the thin filament existing in either an on-or an off-state with calcium and myosin-S1 serving as effectors [Greene and Eisenberg, 1980; Hill et al., 1980; Fraser and Marston, 1995]. This has also been modeled as Tm being in one of three states within a thin filament regulatory unit [McKillop and Geeves, 1993; Maytum et al., 1999]. In either model, the probability of myosin binding to actin is reduced >100 fold in the absence of calcium [Kad et al., 2005]. The rate of myosin binding to the thin filament increases upon calcium binding to troponin. In the three-state model, binding of the first myosin head is slow but necessary to shift the position of Tm, thus increasing the probability of subsequent myosin heads binding to actin by the downstream induction of Tm into the "open" state. This cooperative activation is manifested in vitro both in isometric force measurements [VanBuren et al., 1999] and ATPase rates [Lehrer and Morris, 1984].

*Correspondence to: William H. Guilford, Department of Biomedical Engineering, University of Virginia, Box 800759, Charlottesville, Virginia 22908, USA. guilford@virginia.edu .

The α-isoform of Tm (found in striated muscle) can be phosphorylated, but not the β-isoform [Mak et al., 1978, 1979]. The phosphorylation site of Tm has been verified in multiple species and in both cardiac and skeletal muscle to be near the C-terminus at Ser-283 [Mak et al., 1978]. Recent evidence suggests that a potential kinase for Tm phosphorylation is the ζ isoform of protein kinase C (PKC), but functional studies on the effects of PKC-ζ are not available [Wu and Solaro, 2007]. Studies by Heeley et al. established that Tm phosphorylation was functionally significant in thin filament regulation. Using Tm dephosphorylation from its natively phosphorylated state as a strategy to study regulation, they showed that Tm phosphorylation states affected actin-myosin interactions without affecting actin-Tm binding. Specifically, myosin-S1 ATPase rates were significantly greater when Tm is phosphorylated compared to when it was dephosphorylated [Heeley et al., 1989].

Cooperative activation by myosin was traditionally thought to occur in the "short-range" within a single thin filament regulatory unit (~7 actin monomers, one troponin complex, one tropomyosin) [Bremel and Weber, 1972; Greene and Eisenberg, 1980; Hill et al., 1980, 1983] and as such the cooperative unit size was limited to seven actin monomers or fewer. More recent evidence suggests that the cooperative unit size may extend beyond a thin filament regulatory unit [Geeves and Lehrer, 1994]. Cooperative unit sizes beyond seven actin monomers have been demonstrated to exist in skeletal [Lehrer et al., 1997; Regnier et al., 2002], cardiac [Mirza et al., 2007], and smooth muscle [Marston and Redwood, 1993; Lehrer et al., 1997]. Long-range cooperative activation by myosin-S1 binding has been suggested to extend even longer distances from ~300–500 nm [Vibert et al., 1997] or across the entire length of the thin filament (~1100 nm) [Fraser and Marston, 1995].

Tm is thought to transmit conformational changes (and therefore cooperative activation) over long distances through end-to-end interactions [Edwards and Sykes, 1978, 1980, 1981]. As reported by McLachlan and Stewart [1975], an 8–11 residue overlap exists between the N-C terminus of adjacent Tm molecules, and interactions in the overlap region are charge-dependent [Kay and Bailey, 1960; McLachlan and Stewart, 1975; Sousa and Farah, 2002]. The Tm phosphorylation site is located in this overlap region and may thus play a role in regulating end-to-end interactions. Single residue substitutions at the Ser-283 phosphorylation site show that changing the charge at this residue from a negative charge – as in phosphorylation – to a positive charge significantly weakens end-to-end interactions [Sano et al., 2000]. Structural analysis of the Tm dimer further supports the importance of having strong end-to-end interactions as the C-terminus of the molecule is in a flexible parallel chain conformation as opposed to a coiled-coil [Greenfield et al., 2002, 2003]. As a result, the transmission of conformational changes between subsequent Tm is dependent on stabilizing this pliant end of the protein.

In this study, we investigated the role of Tm phosphorylation in regulation of actomyosin interactions using *in vitro* methods at the level of individual actin filaments interacting with a heavy meromyosin (HMM) coated surface. We measured the force, velocity, and binding of Tm in the phosphorylated and dephosphorylated state when reconstituted on actin filaments. To accomplish this we developed an efficient method using optical trapping to measure the isometric force generated by myosin ensembles. Our data show that dephosphorylation of Tm causes partially reconstituted thin filaments to behave like unregulated actin filaments. We propose that the phosphorylation state of Tm effects the range of cooperative regulation in actomyosin and thus may directly impact the contractile performance of striated muscle.

MATERIALS AND METHODS

Proteins

Myosin was prepared from rat hindleg muscle according to Shiverick et al. [1975] with minor modifications. In brief, 400 mg tissue samples were finely minced and homogenized in an extraction buffer (0.3 M KCl, 10 mM HEPES, 10 mM $Na_4P_2O_7 \cdot 10\ H_2O$, 1 mM $MgCl_2$, 10 mM DTT (dithioreitol), 1 mM ATP, pH 6.8). The homogenate was extracted by stirring at 4° C for 1 h. Following extraction, the supernatant was clarified at 100,000*g* for 1 h at 4°C, and subsequently diluted 3:1 with 10 mM DTT. Myosin was allowed to precipitate for 1 h at 4°C. The precipitate was collected by centrifugation at 4000*g* for 45 min at 4°C and resuspended in storage buffer (0.5 M KCl, 50 mM KH_2PO_4, 3 mM $MgCl_2$, pH 6.8). HMM was extracted from myosin using α-chymotrypsin (Sigma) at a 1:200 dilution for 10 min at room temperature with stirring. The reaction was stopped with PMSF (0.5 mM final concentration in 70% ethanol) for 10 min on ice with stirring. The digestion mixture was then dialyzed against 1 L of buffer containing 25 mM Imidazole/1 mM EGTA, 25 mM KCl, 4 mM $MgCl_2$, and 1 mM DTT, pH 7.4 overnight at 4°C (10 kDa MWCO). The resulting HMM was separated from undigested myosin and LMM by centrifugation at 200,000*g* for 30 min at 4°C, and the pellet discarded.

Actin and α-tropomyosin were extracted from acetone powder attained from rat hindleg muscle. Acetone powder was prepared according to Pardee and Spudich [1982]. Briefly, 20–30 g of rat hindleg tissue was removed and placed on ice for 30 min. The tissue was homogenized in a food processor along with 100 mL of buffer containing 0.15 M KH_2PO_4, 0.1 M KCl, and 1 mM NaN_3, pH 6.5. The homogenate was extracted at 4°C for 10 min with stirring and then centrifuged for 15 min at 1700*g*. The resulting pellet was then extracted twice in 50 mL of buffer containing 50 mM $NaHCO_3$ and 1 mM NaN_3 for 10 min at 4°C followed by centrifugation. The pellet was again extracted in 100 mL of buffer containing 1 mM EDTA and 1 mM NaN_3, pH 7.0 for 10 min at 4°C followed by centrifugation. The extraction process was continued twice with 50 mL of ddH_2O for 5 min at 4°C and five times with 50 mL acetone for 10 min at room temperature. The last three acetone extractions were performed with vacuum-assisted filtration rather than centrifugation. The pellet was allowed to dry overnight on filter paper at room temperature and stored at −20°C.

Actin was extracted from rat hindleg muscle acetone according to Pardee and Spudich [1982] with minor modifications. Acetone powder (250 mg) was extracted in 5 mL of buffer containing 2 mM Tris Base, 0.2 mM ATP, 0.2 mM $CaCl_2$, 1mM NaN_3, and 1mM DTT, pH 8.0 at 0°C for 30 min with mild stirring. The mixture was centrifuged at 4000*g* for 10 min at 4°C and the supernatant was filtered through a glass wool under a light vacuum. The filtered supernatant was polymerized overnight at 4°C by adding at final concentrations 100 mM KCl, 2 mM $MgCl_2$, and 1 mM ATP. The following day, the KCl concentration of the mixture was increased to 0.6 M and stirred for 30 min at 4°C. The solution was then centrifuged at 200,000*g* for 1 h at 4°C. The resulting pellet was resuspended in 750 μL of extraction buffer (above). This solution was dialyzed against 1 L of cold extraction buffer for 48 h with 3–4 buffer changes. The resulting G actin was clarified at 200,000*g* for 1 h at 4°C and subsequently polymerized to F-actin by bringing the solution to final concentrations of 10 mM Imidazole, 0.25 mM EGTA, 25 mM KCl, 4 mM $MgCl_2$, 10 mM DTT, and 1 mM ATP.

α-tropomyosin was prepared from actin acetone powder according to Smillie [1982] with minor modifications. Acetone (500 mg) was extracted with 10 mL of extraction buffer containing 1 M KCl and 0.5 mM DTT, pH 7.0 overnight at room temperature. The extraction mixture was then filtered and the filtrate was saved. The remaining residue was extracted a second time for 2 h at room temperature and the filtrates combined. All subsequent steps were performed at 4° C. The pH of the combined filtrates was decreased to 4.6 for isoelectric precipitation and stirred for 30 min. The suspension was centrifuged at 6000*g* for 20 min to collect the pellet, which

was subsequently resuspended in extraction buffer. The solution was clarified at 6000*g* for 10 min. Isoelectric precipitation was repeated two more times, replacing the extraction buffer with 15 mL of 0.5 mM DTT in the final clarification step. The solution was then precipitated with $(NH_4)_2SO_4$ at 53% saturation while maintaining pH 7.0 and allowed to stand for 30 min. The suspension was clarified at 11,000*g* for 30 min. The supernatant was then precipitated with $(NH_4)_2SO_4$ at a 65% saturation and centrifuged at 11,000*g* for 30 min. The resulting pellet was resuspended in 1.0 mL of 0.5 mM DTT and dialyzed against 1 L of 1 mM DTT.

Protein concentrations were determined using the Advanced Protein Assay Reagent (Cytoskeleton, Denver, CO). Sample purity was assessed with electrophoresis on NuPAGE 4–12% bis-tris gels (Invitrogen, Carlsbad, CA) for myosin and HMM preparations and NuPAGE 12% bis-tris gels (Invitrogen) for thin filament proteins. The phosphorylation state of Tm after purification was determined by large format 2D gel electrophoresis (Bio-Rad). Immobilized pH gradient (IPG) strips with a narrow range (pI = 3.9–5.1) were used for first dimension focusing of Tm. IPG strips were focused for ~45,000 V-h following overnight passive rehydration. Second dimension gel electrophoresis of the focused IPG strips was performed using 17 cm 10–20% Tris-HCl gels run at a constant current of 16 mA for 30 min followed by 24 mA for 5.5 h at 10°C. The gels were subsequently stained using Coomassie blue stain and imaged using an Alpha Innotech FluorChem 8900 imager.

F-actin Biotinylation, Fluorescent Labeling, and Reconstitution with Tm

Fifty microliter of F-actin (2.3 mg/mL) was centrifuged at 200,000*g* for 30 min at 4°C. The resultant pellet was resuspended in 50 μL of biotin labeling buffer consisting of 100 mM HEPES, 2 mM $MgCl_2$, 1 mM ATP, and 1 mM DTT, pH 8.0. NHS-biotin was added at a final concentration of 100 μg/mL. This mixture was allowed to stand for 2 h at room temperature and centrifuged at 200,000*g* for 30 min at 4°C. The resulting pellet was washed three times and resuspended in 20 μL of actin polymerization buffer (100 mM KCl, 25 mM Imidazole, 1 mM EGTA, 1 mM ATP, 1 mM DTT, pH 7.4). The biotinylated F-actin solution was diluted 30:1 in the above actin polymerization buffer and fluorescently labeled with 0.6 nanomoles of TRITC-phalloidin. Tm was bound to actin in this solution by adding a 2.5-fold molar excess of rat skeletal Tm. The final concentration of actin and Tm in the reconstitution mixture was 3 μM and 7.5 μM respectively. This mixture was allowed to stand overnight at 4°C before use.

Actin-Tm reconstitution was verified through cosedimentation. Reconstituted samples were centrifuged at 200,000*g* for 30 min at 4°C. The resulting pellet and supernatant were resuspended in LDS sample buffer (Invitrogen). SDS-PAGE was performed on precast NuPAGE (Invitrogen) 12% bis-tris gels and stained with a Simply Blue Coomassie (Invitrogen) total protein stain. Reconstitution was verified by densitometry such that actin: Tm was approximately 7:1.

Tm Dephosphorylation

Tm dephosphorylation was performed according to Heeley et al [1989]. with minor modifications. Briefly, fluorescently labeled and biotinylated F-actin reconstituted with Tm in its native phosphorylation state was incubated with calf intestine alkaline phosphatase (Calbiochem, San Diego, CA) at an enzyme: Tm molar ratio of 1:100 for 2 h at 37°C. The alkaline phosphatase reaction was stopped by chilling to 4°C. Dephosphorylation was verified using SDS-PAGE and concurrent phosphoprotein and total protein staining was performed on each set of reconstituted proteins ($n = 8$). Gels were washed and fixed before the application of stains. Pro-Q Diamond (Invitrogen) phosphoprotein staining solution was applied to the gels and imaged using a Bio-Rad FX fluorescent scanner. Gels were subsequently stained with Sypro Ruby (Molecular Probes) total protein stain and imaged as above. 16-bit images of each

gel were collected and analyzed using the ImageJ [Rasband, 1997] gel analysis tool. Relative phosphorylation was based on the ratio of phosphoprotein to total protein for the same band.

Actin-Tm Binding

To test the effect of Tm dephosphorylation on actin binding, cosedimentation experiments (explained above) were performed with actin reconstituted with Tm in the natively phosphorylated and dephosphorylated states. Experiments were performed at Tm concentrations ranging from 250 nM–4 μM. The ratio of Tm: actin band densities was calculated and normalized to 4 μM actin-Tm in the natively phosphorylated state (saturating control).

Motility Assay

In vitro motility was performed at 30°C at 1 mM ATP as previously described [Guo and Guilford, 2004; Rao et al., 2007; Snook et al., 2008]. In brief, HMM in actin buffer (25 mM KCl, 25 mM Imidazole, 1 mM EGTA, 4 mM $MgCl_2$, 10 mM DTT, pH 7.4) was flowed into a flow cell constructed from a nitrocellulose coverslip and glass slide spaced by two mylar shims. HMM was applied at a concentration range of 5–200 μg/mL for HMM head density experiments. After 1 min of incubation, the flow cell was blocked with 1% BSA in low salt actin buffer for 1 min. Following an actin buffer wash, either bare actin, actin with natively phosphorylated Tm (A+Tm.P), or actin with dephosphorylated tropomyosin (A+Tm.DP) labeled with TRITC phalloidin was diluted in actin buffer 100:1 and added to the flow cell and incubated for 1 min. Two actin buffer washes followed and a low salt motility buffer (25 mM KCl, 25 mM Imidazole, 1 mM EGTA, 4 mM $MgCl_2$, 10 mM DTT, 1 mM ATP, 0.5% methylcellulose, pH 7.4) including an oxygen scavenger (0.125 mg/mL glucose oxidase, 0.0225 mg/mL catalase, 2.87 mg/mL glucose) was applied to the flow cell. The flow cell was pre-heated for 1 min. at 30°C and placed on a IX70 fluorescence microscope (Olympus, Center Valley, PA) with a heated microscope objective and images captured with an intensified CCD camera (PTI, Birmingham, NJ) and LG3 video capture card (Scion, Frederick, MD). Actin filaments were tracked using a custom centroid-based recursive segmentation and tracking algorithm [Snook et al., 2008] which is available from the authors upon request as a software plugin for ImageJ [Rasband, 1997].

Measuring Stall Force Using a Laser Trap Transducer

As a physiologically-relevant measure of the force production in the purified actomyosin system, an optical trap assay was developed to measure the stall force of multiple myosin molecules interacting with an actin filament. Traditionally the stall force of actomyosin is measured using a microneedle approach [VanBuren et al., 1994, 1999; Kishino and Yanagida, 1988; Homsher et al., 2000; Clemmens and Regnier, 2004; Clemmens et al., 2005] In that approach, a fluorescently labeled actin filament is bound to the tip of a glass microneedle of known stiffness. The actin filament is brought into contact with a motility surface coated with myosin or HMM. As myosin pulls on actin, the microneedle is bent to an extent where the force on the microneedle exactly opposes the force generated by myosin. This measure is analogous to measurements of isometric force in muscle fibers, but can be performed in simplified molecular systems. However, there are two important limitations to this otherwise powerful method. First, throughput is limited due to the complicated procedure for calibration and use of the microneedles. Second, it is difficult to measure the length of the filament that is in physical contact with the motility surface because the microneedle must remain out of contact with the coverslip.

We replaced the glass microneedle with an optically trapped, streptavidin-coated bead. The bead was bound to the trailing end of a motile biotinylated actin filament; the bead was subsequently displaced from trap center as the filament moved (Fig. 1). Because laser traps

behave like Hookean springs over short distances, displacement of the bead caused an increasing force to be applied to the actin filament until it reached stall. Knowing the trap stiffness and the displacement of the bead from trap center, one is able to calculate the stall (isometric) force generated by the myosin. This comparatively high-throughput approach allowed us to measure stall forces at lower myosin concentrations than are typically possible with the microneedle approach. Further, the entire length of the actin filament is in contact with the surface and can be measured easily and accurately, since the trapped bead and the actin filament are in the same focal plane.

Details of our laser trap have been described previously [Guilford et al., 2004], except that the laser has been replaced with a 1090 nm fiber laser (SPI, Southhampton, UK), and the CCD camera with a SIT camera (Dage-MTI, Michigan City, IN) for fluorescence imaging. Back focal plane interferometry was used to determine the displacement of a trapped bead relative to the trap center. Detector and trap stiffness calibrations were performed using the step response method [Svoboda and Block, 1994; Dupuis et al., 1997] and confirmed using power spectral density [Allersma et al., 1998]. Step response calibrations were performed 2.6 bead radii above the surface of the flow cell to avoid unwanted protein-protein interactions and to minimize the near-wall drag effects.

Fluorescent beads were prepared from 0.97 μm streptavidin-coated microspheres (Bangs Laboratories, Fishers, IN). Initially, a 40 μL suspension of beads was washed and pelleted two times in 1 mL of actin buffer (25 mM Imidazole, 1 mM EGTA, 25 mM KCl, 4 mM $MgCl_2$, pH 7.4). The beads were then resuspended in 200 μL of actin buffer and 10 μL of TRITC-labeled BSA (10 mg/mL) in actin buffer. This mixture was allowed to incubate at 4°C for 30 min. The fluorescent beads were washed three times with BSA in actin buffer (1 mg/mL) and resuspended in 200 μL of the same solution. The fluorescent bead suspension was good for up to 2 weeks.

Flow cells were constructed from one plain and one nitrocellulose-coated microscope cover slip as previously described [Guilford et al., 1997; Guo and Guilford, 2004], except that no glass microspheres were included beneath the nitrocellulose. HMM was applied to flow cells at concentrations of 10, 15, 20, 35 or 50 μg/mL followed by a 1 min incubation. The surface was subsequently blocked with 1 mg/mL BSA followed by a 1 min incubation. TRITC-phalloidin labeled actin filaments were then added along with biotinylated microspheres (above), 100 μM ATP, and 600 nM free natively phosphorylated Tm (Tm.P) or dephosphorylated Tm (Tm.DP). The filaments were either (1) bare actin, (2) A+Tm.P, or (3) A+Tm.DP. Free Tm was included to maintain Tm binding to actin as in previous studies [VanBuren et al., 1999; Homsher et al., 2000], but at a significantly higher concentration.

The flow cells were placed on a piezoelectric microscope stage. Individual fluorescent beads were trapped and a motile actin filament was chosen. Long, straight filaments were preferentially chosen. A trapped bead was brought into contact with the trailing end of the motile filament by moving the piezoelectric stage (refer to Fig. 1). A stall force event was recorded when the bead bound to the actin filament and caused the filament to stop. The data trace showed this event with a gradual increase in the displacement signal followed by a plateau period indicating the filament has stalled. Stall periods lasting >100 ms were recorded as true stalls. The event ended when the stalled actin filament broke, leaving a small portion of the filament still attached to the bead. This was seen in the displacement signal as a step decrease. Stall force events required both visual confirmation and evidence in the data trace before they were counted. At times, the actin filaments did not detach from the streptavidin bead and instead detached from the myosin heads on the surface that had stopped cycling. However, data traces for such events that demonstrated a gradual rise in displacement followed by a plateau and step decrease were included as stall events as well. Bead-filament attachment events followed by

a gradual decline in displacement were not considered true stall events. Occasionally, multiple stall events would occur on the same stalled filament indicating multiple bond formations and breaks between biotins on the actin filaments and streptavidin on the beads. Only the final stall event was recorded as the true stall event. Figure 2 shows a representative stall event data trace collected using this method. Stall force measurements were repeated over a range of actin filaments lengths (1–7 μm). Actin filament lengths were determined manually by directly measuring the filament length on the video monitor and multiplying the resulting length by a calibration factor for the screen. The actin filament length measurements were accurate within ±250 nm. All length measurements were taken from the center of the fluorescent streptavidin bead to the end of the actin filament. A 500 nm distance was subtracted from the initial measurement to account for the radius of the streptavidin bead. The number of HMM heads that may have interacted with each actin filament was estimated from HMM density measurements [Guo and Guilford, 2004] as the product of the HMM head density at the given HMM concentration, the measured actin filament length, and the estimated maximum distance from which a given HMM may bind the actin filament [Toyoshima et al., 1989;Uyeda et al., 1990]. We assumed this “interaction distance” to be 20 nm, or 10 nm from either side of the filament center, though one can argue for greater or smaller distances based on the dimensions of myosin heads, the filament width, and geometric constraints.

Stall force data was collected as voltage-time data at a sampling frequency of 1 kHz. *X*- and *y*-axis voltage versus time traces were collected and the force vector magnitude was calculated at every time point using custom software and the Pythagorean theorem. Force was estimated by multiplying the resultant magnitude with the displacement calibration and trap stiffness.

Statistical Analysis

Sample number (n) in all cases except force measurements was taken as the number of replicate experiments, not the measured number of actin filaments. Each replicate experiment used in the in vitro motility assay represented >500 individual filaments measured per experimental condition described. Five replicate experiments were performed for each experimental condition. Actin-Tm binding ratios and filament velocities were both normalized against daily controls. Significance was determined by z-test and $P < 0.05$. All errors were calculated as standard error of the mean (s.e.m.).

Force data was fit by linear regression using Microsoft Excel®. Significant differences between fits were determined using a z-statistic based upon the slope of the regression (*m*) and the standard error (*se*) of the fit for *m*: $z = |m_1 - m_2| / \sqrt{se_1^2 + se_2^2}$

RESULTS

Tm Phosphorylation Does Not Effect Tm Binding to Actin

Tm purified from rat skeletal muscle acetone powder was endogenously phosphorylated (Fig. 3). Tm dephosphorylation by alkaline phosphatase was clearly evident through phosphoprotein staining and isoelectric focusing. The fraction of Tm in the Tm.P state after purification was determined to be 72% by 2D gel electrophoresis of phosphorylated samples. However, the true native level of phosphorylation is presumably higher as endogenous phosphatases will reverse some of the native phosphorylation during protein extraction. In terms of double-stranded Tm molecules, this would mean at least one strand is phosphorylated ~92% of the time and both strands phosphorylated 53% of the time if we assume that there is no preferential dimerization of phosphorylated or dephosphorylated Tm molecules. Gel analysis of the phosphoprotein images showed a ninefold decrease in Tm phosphorylation after treatment with alkaline phosphatase. Binding ratios of Tm.P and Tm.DP to actin was measured by densitometry to be

0.18 ± 0.05 (n = 8) and 0.15 ± 0.04 (n = 8) Tm/actin (mol/mol). These values are both near the expected molar ratio of 7 actin: 1 Tm (0.14 mol/mol).

Actin-Tm cosedimentation experiments (n = 6) were performed to determine the effect of Tm dephosphorylation on actin binding. Previous work from another group showed that actin binding is not affected by Tm dephosphorylation [Heeley et al., 1989]. Similarly, our cosedimentation experiments showed no difference in the K_ms for Tm binding to actin of 951 ± 40 nM and 927 ± 32 nM for Tm.P and Tm.DP, respectively. These values fall within the range of previously published K_m for Tm binding to actin [Heeley et al., 1989; Hill et al., 1992; Moraczewska and Hitchcock-DeGregori, 2000; Sano et al., 2000; Singh and Hitchcock-DeGregori, 2006] The data also suggested cooperative binding of Tm to actin (Fig. 4) as seen in a number of studies [Heeley et al., 1989; Moraczewska and Hitchcock-DeGregori, 2000; Sano et al., 2000; Singh and Hitchcock-DeGregori, 2006]. The corresponding Hill coefficients for A+Tm.P and A+Tm.DP were significantly different at 2.1 ± 0.2 and 2.9 ± 0.3, respectively.

Tm Dephosphorylation Does Not Effect Sliding Velocity

The unloaded sliding velocity of bare actin, A+Tm.P, and A+Tm.DP was measured over a range of HMM loading concentrations (5–200 μg/mL). The overall velocities were measured as the product of the mean velocities of motile filaments and the fraction of moving filaments (Fig. 5). A+Tm.P filaments were propelled at a slightly but significantly greater overall velocity (4.1 ± 0.1 μm/s) than both bare actin (3.7 ± 0.2 μm/s) and A+Tm.DP (3.3 ± 0.2 μm/s) filaments based on the fitted values for V_{max}. Bare actin also showed a slight increase in V_{max} compared to A+Tm.DP filaments. Similar to VanBuren et al. [1999], the presence of tropomyosin on actin filaments nearly abolished sliding velocities at low HMM loading densities (5–10 μg/mL) independent of Tm phosphorylation state. Sliding velocities for Tm-decorated filaments rose at a slower rate than bare actin filaments. The HMM loading concentrations at half-maximal velocity for bare actin, actin-NP Tm, and actin-DP Tm were 5.9 ± 0.7 μg/mL, 17.9 ± 0.6 μg/mL, and 18.0 ± 1.0 μg/mL, respectively.

Tm Phosphorylation Increases Stall Force

An optical trap assay was utilized to estimate the stall force of bare actin and actin reconstituted with Tm.P and Tm.DP. Force was plotted as a function of filament length (Fig. 6) and also as a function of the number of available HMM heads at HMM loading concentrations of 10, 15, 20, 35, and 50 μg/mL. These HMM loading concentrations were related to the HMM surface densities given in Table I based on NH_4-ATPase data from our lab [Guo and Guilford, 2004]. The isometric "stall" force of all five conditions was analyzed as force per actin filament length (f_{length}) as in previous studies [Van-Buren et al., 1994,1999;Homsher et al., 2000;Clemmens et al., 2005]. Table I lists the corresponding f_{length} values for all fifteen conditions. Our f_{length} values using bare actin and A+Tm.P filaments are in close agreement with the values reported by VanBuren et al. [1999]. The results of bare actin and A+Tm.P also agree with earlier findings that suggest cooperative binding of myosin to actin-Tm and non-cooperative binding of myosin to bare actin [VanBuren et al., 1999]. Of the three regulatory states, A+Tm.P produced the lowest f_{length} at the low HMM concentration (10 μg/mL), and the highest f_{length} at the intermediate HMM concentrations of 15, 20, 35 μg/mL. At 50 μg/mL of HMM, all cases begin to converge to a common f_{length} (Fig. 7A). Interestingly, A+Tm.DP is statistically indistinguishable from bare actin with regards to f_{length} at any concentration.

The average force per HMM head (f_{head}) was estimated as the ratio of the total force produced by a filament and the number of HMM heads available over the length of the filament (see Table II). For comparison to previous work, bare actin over an intermediate HMM concentration of 20 μg/mL produced a f_{head} of 0.21 ± 0.01 pN/head. Work by others using the microneedle technique produced a similar f_{head} of 0.2 pN/head for skeletal muscle actomyosin

[VanBuren et al., 1994]. At intermediate HMM concentration of 20 μg/mL, force was increased ~50% in A+Tm.P (Fig. 7B), but was unchanged relative to bare actin in A+Tm.DP (0.18 ± 0.02 pN/head). At a HMM concentration of 10 μg/mL, the f_{head} trend showed the opposite effect; the force production of bare actin and A+Tm.DP increased ~80% relative to A+Tm.P. However at the highest HMM concentration of 50 μg/mL, the differences in force per head disappear between all cases (See Fig. 7B).

DISCUSSION

Our data show that the phosphorylation state of Tm has dramatic effects on the force generation of partially reconstituted thin filaments. Specifically, Tm appears to enhance cooperative activation of the actin filament by myosin [Goldman et al., 1984; Palmiter et al., 1996; Swartz et al., 1996; VanBuren et al., 1999; Clemmens et al., 2005] beyond the length of a single thin filament regulatory unit in the in vitro motility assay, but only when phosphorylated. This enhanced cooperativity is probably related to strengthened end-to-end interactions on the Tm polymer that allow adjacent Tm monomers to move as a unit when myosin binds [McLachlan and Stewart, 1975; Edwards and Sykes, 1978, 1980, 1981; Heeley et al., 1989; Sano et al., 2000]. Additionally, stall forces at intermediate HMM concentrations increase significantly when Tm is phosphorylated. This suggests that Tm may have phosphorylation-dependent effects on actin or myosin apart from steric hindrance that may influence force production.

Cooperative Activation

In a non-cooperative system, one would expect the f_{length} (force per unit length) of actin filament to be proportional to the density of myosin heads (or HMM) on the surface, [HMM], since this would leave more myosin heads in a position to bind to the filament and generate force. However, because there are discrete binding sites for myosin on actin, f_{length} should obey simple saturable binding kinetics,

$$f_{\text{length}}([\text{HMM}]) = \frac{f_{\text{length,max}} \times [\text{HMM}]^n}{K_f^n + [\text{HMM}]^n} \quad (1)$$

where $f_{length,max}$ is the force per unit length at saturating HMM density, K_f is the HMM concentration to achieve half maximal force, and n is the Hill coefficient. Both K_f and [HMM] have units of molecules/μm^2. The isometric force data for bare actin and A+Tm.DP are well fit by this model when n = 1 (simple saturable binding), with fitted K_f of 1600 ± 210 heads/μm^2 and 1650 ± 240 heads/μm^2 and $f_{length,max}$ of 13.1 ± 2.6 pN/μm and 12.6 ± 3.9 pN/μm respectively. The data for A+Tm.P, in contrast, is fitted with a K_f of 1020 ± 20 heads/μm^2 and n of 2.7 ± 0.1. This is highly suggestive of cooperative binding of myosin to the partially reconstituted thin filament, but only when Tm is phosphorylated. When the data for A+Tm.P was forced to a non-cooperative (n = 1) condition, the resulting curve did not fit the data, further demonstrating the cooperative nature of partially reconstituted thin filaments with phosphorylated Tm.

One may also express these data as the time-averaged isometric force generated by each myosin head, f_{head}.f_{head} and f_{length} are related by

$$f_{\text{head}}([\text{HMM}]) = f_{\text{length}}([\text{HMM}])/(w \times ([\text{HMM}])) \quad (2)$$

where w is the width of the "band" along the actin filament within which a myosin might interact with actin (assumed to be 20 nm). These data are shown in Fig. 7B, and make clear that the force per head one measures depends upon the HMM (myosin) concentration. This is

because myosin binds saturably to actin, and therefore not all myosins within the "band" will successfully bind to actin, though Eq. 2 assumes they do. Substituting (1) into (2) we find

$$f_{\text{head}}([\text{HMM}]) = \frac{f_{\text{length,max}} \times [\text{HMM}]^{n-1}}{w \times (K_f^n + [\text{HMM}]^n)} \quad (3)$$

The f_{head} data was well fitted by this model which accurately represents the biphasic f_{head} found for A + Tm.P (Fig. 7B).

What value, then, is an accurate representation of f_{head} if it is concentration-independent? Consider $n = 1$ and $[HMM] = 0$. Eq. 3 reduces to

$$f_{\text{head}}^{o} = f_{\text{length,max}} / (w \times K_f) \quad (4)$$

This measure of force per head is concentration-independent and can therefore also be easily compared between studies. For our bare actin data, we find f_{head}^{0} to be 0.41 pN and our A +Tm.DP filaments to be 0.38 pN. When f_{length} values reported by Van Buren et al. [1999] were fit to Eq. 1, the resulting f_{head}^{0} was estimated to be 0.48 pN—in close agreement with our measured values. These measurements of time averaged force/HMM head (~0.4 pN) in no way conflict with existing data on the unitary force of a single HMM heads measured using single molecule techniques. The time-averaged force of a single head includes both attached and detached times of HMM to actin, unlike single-molecule approaches where only the attached time is considered. If we assume a unitary force of 3.5 pN [Guilford et al., 1997], we simply predict a duty ratio near stall of ~0.12—not unexpected for fast motors like striated muscle myosins.

Based on our estimate of 0.41 pN per head and a stall force of ~30 pN for a 5 μm filament (measured in the phosphorylated "cooperative" condition), we estimate 73 force-generating heads, or one head for every 1.8 Tm in a groove. This is close to one head per full repeat of the actin filament. This value is not surprising given the geometry of the motility assay where only one or two myosin binding sites face the myosin-coated surface every half-repeat of the actin filament. We expect in our experiments that cooperative activation within a single thin filament regulatory unit exists independent of Tm phosphorylation but remains "hidden" due limited myosin-binding site accessibility. If cooperative displacement of end-to-end linked Tm by myosin promotes subsequent myosin binding, we might expect this to occur at sub-saturating myosin densities when there is one head bound for every 2 Tm in a groove, as we found (above). It is reasonable to conclude that binding of a head can cooperatively activate a regulatory unit and at least one of its neighbors.

An obvious, alternative explanation to cooperativity for the difference between Tm.P and Tm.DP would be that Tm.DP dissociates from the actin filament. However, we verified data from another group that Tm binding to actin remains unchanged regardless of the phosphorylation state [Heeley et al., 1989]. Further, it has been established that Tm binding domains to actin are not located on or near the Tm phosphorylation site at the carboxy terminus of the molecule [Mak et al., 1978; Singh and Hitchcock-DeGregori, 2003, 2006; Hitchcock-DeGregori et al., 2007].

Force Production and Crossbridge Kinetics

From a mechanical viewpoint, a simplified cycle of actomyosin function can be described by two states in which myosin is either detached from actin, or attached and generating its unitary

force (F) or displacement (d). The fraction of the total cycle in which the cross bridge is attached and generating force or motion is defined as its duty cycle,

$$f = t_{on}/(t_{on}+t_{off}) \tag{5}$$

where t_{on} is the time myosin spends attached to actin, t_{off} is the time spent detached, and (t_{on} + t_{off}) is the total cycle time. Since force generation by a single cross-bridge occurs in discrete events, one can estimate the cross-bridge force averaged over the entire cycle (F_{avg}) as the product of the unitary force and duty cycle,

$$F_{avg} = F \times f \tag{6}$$

which should be reflected by the stall force measured in our study. Similarly, the velocity with which actin is propelled, V_{actin}, is directly proportional to the step displacement, d, and inversely related to the attached time, t_{on}. Intuitively, if each step myosin takes requires less time, then those steps may be placed closer in time, resulting in an increased velocity.

$$V_{actin} \approx d/t_{on} \tag{7}$$

If we assume that neither the step displacement nor the unitary force change between the phosphorylated and dephosphorylated states of Tm, then the kinetics of transitions between the attached and detached states of myosin must be effected. At an intermediate HMM surface density of 1255 heads/μm^2, we observe a 53% increase in stall force (proportional to F_{avg}), but a small change in Vactin comparing A+Tm.P to A+Tm.DP. The increased force from A +Tm.P compared to bare actin is consistent with the work of VanBuren et al. [1999]. Based on Eq. 5–Eq. 7, the detachment rate ($1/t_{on}$) must be little changed between the two Tm phosphorylation states to explain our velocity data. Thus the attachment rate ($1/t_{off}$) must be increased when Tm is phosphorylated. These data are not completely consistent with the results of Heeley et al. [1989] who showed an approximate 22% increase in actin-activated ATPase rate (an 18% reduction in cycle time, $t_{on} + t_{off}$) when Tm was phosphorylated. However, Heeley was able to separate phosphorylated from dephosphorylated Tm, so the relative effects could easily have been greater than we measured.

The effects of tropomyosin phosphorylation on enhanced cooperative activation by myosin may be explained by end-to-end interactions, but question remains how actin-NP Tm is able to produce a greater force than unregulated actin filaments at intermediate HMM concentrations. Similar effects were observed by Van Buren et al. [1999] using the microneedle force assay, and by Lehrer and Morris [1984] using ATPase measurements. These data are not explained by models of regulation that incorporate only steric hindrance of myosin binding. We consider it unlikely that Tm phosphorylation will directly effect myosin step size or unitary force production considering that the position of Tm on the actin filament does not place it range of the myosin lever domain. Two-headed coordination of myosin heads [Kad et al., 2005] may also be ruled out as the HMM used in our experiments were bound to the motility surface by one head leaving only the other head available for interaction [Guo and Guilford, 2004].

The simplest explanation for this increase in force is that Tm accelerates stereospecific myosin binding to actin resulting in an increased duty cycle (see Eq. 5). This could be the result of a direct interaction between myosin and Tm, or through an influence of Tm on the structure of the actin filament. As an actin-binding protein, Tm has a significant role in the maintaining the stability of the actin filament, with seven quasi-equivalent binding sites along the whole length

of the molecule [McLachlan and Stewart, 1976;Phillips, 1986]. Tm also increases the stiffness [Kojima et al., 1994] and the flexural rigidity [Greenberg et al., 2008] of the actin filament. It is not known, however, if Tm binding induces subtle but important structural changes in F-actin. Single molecule force spectroscopy studies [Guo and Guilford, 2006] can detect very small conformational changes in protein binding interfaces, and may provide additional insight.

Potential Role for Tm Phosphorylation in Regulation of Striated Muscle Contraction

The phosphorylation state of Tm may have a significant role in the regulation of contraction. Tm phosphorylation is associated with cytoskeletal remodeling in response to oxidative stress [Houle et al., 2003]. Further, Tm phosphorylation increases 150% over control during remote zone left ventricular dysfunction (RZLVD), a contractile disorder that occurs after myocardial infarction, but in regions of the left ventricle that do not experience ischemia. This increase in phosphorylation coincides with a small but significant increase in the velocity of purified thin filaments over myosin in the in vitro motility assay [Rao et al., 2007]. Taken together, these results suggest that Tm phosphorylation may serve as a compensatory mechanism that attempts to upregulate contractile function when myosin activity is significantly reduced. In addition, recent evidence from “heavy” Tm isoforms in *Drosophila melanogaster* suggests that phosphorylation in the C-termini may be related to the regulation of stretch activation in indirect flight muscle [Mateos et al., 2006].

Whereas contractile perturbations may induce Tm phosphorylation and upregulation of force production, the opposite has been reported when the ability to phosphorylate Tm is taken away. Using a transgenic mouse model, the last nine residues in the C-terminus of α-Tm were substituted with that of nonphosphorylatable β-Tm in cardiac muscle. The chimera dramatically reduced contractility, the rates of contraction and relaxation, and left ventricular peak pressure [Gaffin et al., 2006]. These results show that basic cardiac muscle function is substantially impaired when native levels of phosphorylation in Tm are not attained. Transgenic mouse studies of involving the MAP kinase signaling cascade have also demonstrated that dephosphorylation of α-Tm is associated with depressed myocardial sarcomeric tension and ATPase activity [Vahebi et al., 2007].

Thus far, we have been able to demonstrate using rat skeletal isoforms of α-Tm and myosin that Tm phosphorylation states impact the cooperativity and level of force production in actomyosin interactions. Rabbit cardiac α-Tm, however, may be more heavily phosphorylated (~2.3×) than skeletal muscle Tm [Mak et al., 1978], suggesting that Tm phosphorylation may have much larger physiological consequences in myocardium than in skeletal muscle. Indeed, the propagation of cooperative activation may be especially important in cardiac muscle since a fairly small change in the number of strongly bound crossbridges causes large changes in calcium sensitivity of force and crossbridge kinetics [Metzger, 1995; Fitzsimons and Moss, 1998; Fitzsimons et al., 2001]. Thus the magnitude of these effects may be linked to the phosphorylation level of tropomyosin in cardiac muscle.

Limitations

There are limitations both to our laser trap assay and our biochemical approach to studying Tm phosphorylation. Optical trapping is limited in the amount of resistance that can be applied against a moving filament. We are thus restricted to a somewhat lower register of forces compared to the traditional microneedle assay. Further, as with the microneedle assay the number of myosin heads that are bound to a given filament can only be estimated. Finally, owing to the similarity in isoelectric points between Tm and troponin T (TnT) in the rat, there is some contamination of Tm with TnT in our preparations. PKC-induced TnT phosphorylation has potential calcium-dependent regulatory effects in cardiac muscle in the presence of troponin I [Mazzei and Kuo, 1984]. However, in our preparations native TnT phosphorylation

was low, and there was no TnI present. Therefore, we do not believe TnT copurification significantly interfered with our results.

Ultimately, manipulation of the full range of Tm phosphorylation will be necessary to understand its role in thin filament regulation. Although the kinase for Tm remains elusive, there are potential candidates, including PKC-ζ [Wu and Solaro, 2007]. Also, a motif scan for phosphorylation sites on rat skeletal muscle α-Tm using the Scansite utility [Obenauer et al., 2003] suggests that Ser-283 may be surrounded by a protein kinase D (PKD, also known as PKC-μ) phosphorylation motif. In addition to increased PKC activity, increased PKD expression has been observed in heart failure. PKC activity has been associated with reduced Ca^{2+} sensitivity but not maximal tension in cardiomyocytes. It is not known whether PKC- and PKD-mediated phosphorylation is detrimental to cardiac function or represents another mechanism to maintain cardiac relaxation rates [Hamdani et al., 2008].

Acknowledgments

The authors would like to thank the laboratories of Dr. Thomas Skalak and Edward Botchwey for providing animal tissues and the Cardiovascular Research Center and the Department of Biomedical Engineering at the University of Virginia for scholarly support. The authors would also like to thank the laboratory of Dr. Michael Regnier at the University of Washington for Tm purification protocols and helpful discussions.

REFERENCES

Allersma MW, Gittes F, deCastro MJ, Stewart RJ, Schmidt CF. Two-dimensional tracking of ncd motility by back focal plane interferometry. Biophys J 1998;74:1074–1085. [PubMed: 9533719]

Bremel RD, Weber A. Cooperation within actin filament in vertebrate skeletal muscle. Nat New Biol 1972;238:97–101. [PubMed: 4261616]

Clemmens EW, Regnier M. Skeletal regulatory proteins enhance thin filament sliding speed and force by skeletal HMM. J Muscle Res Cell Motil 2004;25:515–525. [PubMed: 15711882]

Clemmens EW, Entezari M, Martyn DA, Regnier M. Different effects of cardiac versus skeletal muscle regulatory proteins on in vitro measures of actin filament speed and force. J Physiol 2005;566:737–746. [PubMed: 15905219]

Dupuis DE, Guilford WH, Wu J, Warshaw DM. Actin filament mechanics in the laser trap. J Muscle Res Cell Motil 1997;18:17–30. [PubMed: 9147990]

Edwards BF, Sykes BD. Assignment and characterization of the histidine resonances in the 1H nuclear magnetic resonance spectra of rabbit tropomyosins. Biochemistry 1978;17:684–689. [PubMed: 623737]

Edwards BF, Sykes BD. Nuclear magnetic resonance evidence for the coexistence of several conformational states of rabbit cardiac and skeletal tropomyosins. Biochemistry 1980;19:2577–2583. [PubMed: 7397090]

Edwards BF, Sykes BD. Analysis of cooperativity observed in pH titrations of proton nuclear magnetic resonances of histidine residues of rabbit cardiac tropomyosin. Biochemistry 1981;20:4193–4198. [PubMed: 7284320]

Fitzsimons DP, Moss RL. Strong binding of myosin modulates length-dependent Ca2+ activation of rat ventricular myocytes. Circ Res 1998;83:602–607. [PubMed: 9742055]

Fitzsimons DP, Patel JR, Moss RL. Cross-bridge interaction kinetics in rat myocardium are accelerated by strong binding of myosin to the thin filament. J Physiol 2001;530:263–272. [PubMed: 11208974]

Fraser ID, Marston SB. In vitro motility analysis of actin-tropomyosin regulation by troponin and calcium. The thin filament is switched as a single cooperative unit. J Biol Chem 1995;270:7836–7841. [PubMed: 7713874]

Gaffin RD, Gokulan K, Sacchettini JC, Hewett TE, Klevitsky R, Robbins J, Sarin V, Zawieja DC, Meininger GA, Muthuchamy M. Changes in end-to-end interactions of tropomyosin affect mouse cardiac muscle dynamics. Am J Physiol Heart Circ Physiol 2006;291:H552–H563. [PubMed: 16501024]

Geeves MA, Lehrer SS. Dynamics of the muscle thin filament regulatory switch: The size of the cooperative unit. Biophys J 1994;67:273–282. [PubMed: 7918995]

Goldman YE, Hibberd MG, Trentham DR. Relaxation of rabbit psoas muscle fibres from rigor by photochemical generation of adenosine-5′-triphosphate. J Physiol 1984;354:577–604. [PubMed: 6481645]

Greenberg MJ, Wang CL, Lehman W, Moore JR. Modulation of actin mechanics by caldesmon and tropomyosin. Cell Motil Cytoskeleton 2008;65:156–164. [PubMed: 18000881]

Greene LE, Eisenberg E. Cooperative binding of myosin subfragment-1 to the actin-troponin-tropomyosin complex. Proc Natl Acad Sci USA 1980;77:2616–2620. [PubMed: 6930656]

Greenfield NJ, Palm T, Hitchcock-DeGregori SE. Structure and interactions of the carboxyl terminus of striated muscle alpha-tropomyosin: It is important to be flexible. Biophys J 2002;83:2754–2766. [PubMed: 12414708]

Greenfield NJ, Swapna GV, Huang Y, Palm T, Graboski S, Montelione GT, Hitchcock-DeGregori SE. The structure of the carboxyl terminus of striated alpha-tropomyosin in solution reveals an unusual parallel arrangement of interacting alpha-helices. Biochemistry 2003;42:614–619. [PubMed: 12534273]

Guilford WH, Dupuis DE, Kennedy G, Wu J, Patlak JB, Warshaw DM. Smooth muscle and skeletal muscle myosins produce similar unitary forces and displacements in the laser trap. Biophys J 1997;72:1006–1021. [PubMed: 9138552]

Guilford WH, Tournas JA, Dascalu D, Watson DS. Creating multiple time-shared laser traps with simultaneous displacement detection using digital signal processing hardware. Anal Biochem 2004;326:153–166. [PubMed: 15003556]

Guo B, Guilford WH. The tail of myosin reduces actin filament velocity in the in vitro motility assay. Cell Motil Cytoskeleton 2004;59:264–272. [PubMed: 15505809]

Guo B, Guilford WH. Mechanics of actomyosin bonds in different nucleotide states are tuned to muscle contraction. Proc Natl Acad Sci USA 2006;103:9844–9849. [PubMed: 16785439]

Hamdani N, Kooij V, van Dijk S, Merkus D, Paulus WJ, Remedios CD, Duncker DJ, Stienen GJ, van der Veldon J. Sarcomeric dysfunction in heart failure. Cardiovasc Res 2008;77:649–658. [PubMed: 18055579]

Heeley DH, Watson MH, Mak AS, Dubord P, Smillie LB. Effect of phosphorylation on the interaction and functional properties of rabbit striated muscle α α-tropomyosin. J Biol Chem 1989;264:2424–2430. [PubMed: 2521628]

Hill TL, Eisenberg E, Greene L. Theoretical model for the cooperative equilibrium binding of myosin subfragment 1 to the actin-troponin-tropomyosin complex. Proc Natl Acad Sci USA 1980;77:3186–3190. [PubMed: 10627230]

Hill TL, Eisenberg E, Greene LE. Alternate model for the cooperative equilibrium binding of myosin subfragment-1-nucleotide complex to actin-troponin-tropomyosin. Proc Natl Acad Sci USA 1983;80:60–64. [PubMed: 6572009]

Hill LE, Mehegan JP, Butters CA, Tobacman LS. Analysis of troponin-tropomyosin binding to actin. Troponin does not promote interactions between tropomyosin molecules. J Biol Chem 1992;267:16106–16113. [PubMed: 1644797]

Hitchcock-DeGregori SE, Greenfield NJ, Singh A. Tropomyosin: Regulator of actin filaments. Adv Exp Med Biol 2007;592:87–97. [PubMed: 17278358]

Homsher E, Lee DM, Morris C, Pavlov D, Tobacman LS. Regulation of force and unloaded sliding speed in single thin filaments: Effects of regulatory proteins and calcium. J Physiol 2000;524(Part 1):233–243. [PubMed: 10747195]

Houle F, Rousseau S, Morrice N, Luc M, Mongrain S, Turner CE, Tanaka S, Moreau P, Huot J. Extracellular signal-regulated kinase mediates phosphorylation of tropomyosin-1 to promote cytoskeleton remodeling in response to oxidative stress: Impact on membrane blebbing. Mol Biol Cell 2003;14:1418–1432. [PubMed: 12686598]

Kad NM, Kim S, Warshaw DM, VanBuren P, Baker JE. Single-myosin crossbridge interactions with actin filaments regulated by troponin-tropomyosin. Proc Natl Acad Sci USA 2005;102:16990–16995. [PubMed: 16287977]

KAY CM, Bailey K. Light scattering in solutions of native and guanidinated rabbit tropomyosin. Biochim Biophys Acta 1960;40:149–156. [PubMed: 14404979]

Kishino A, Yanagida T. Force measurements by micromanipulation of a single actin filament by glass needles. Nature 1988;334:74–76. [PubMed: 3386748]

Kojima H, Ishijima A, Yanagida T. Direct measurement of stiffness of single actin filaments with and without tropomyosin by in vitro nanomanipulation. Proc Natl Acad Sci USA 1994;91:12962–12966. [PubMed: 7809155]

Lehrer SS, Morris EP. Comparison of the effects of smooth and skeletal tropomyosin on skeletal actomyosin subfragment 1 ATPase. J Biol Chem 1984;259:2070–2072. [PubMed: 6230348]

Lehrer SS, Golitsina NL, Geeves MA. Actin-tropomyosin activation of myosin subfragment 1 ATPase and thin filament cooperativity. The role of tropomyosin flexibility and end-to-end interactions. Biochemistry 1997;36:13449–13454. [PubMed: 9354612]

Mak A, Smillie LB, Barany M. Specific phosphorylation at serine-283 of alpha tropomyosin from frog skeletal and rabbit skeletal and cardiac muscle. Proc Natl Acad Sci USA 1978;75:3588–3592. [PubMed: 278975]

Mak AS, Lewis WG, Smillie LB. Amino acid sequences of rabbit skeletal β- and cardiac tropomyosins. FEBS Lett 1979;105:232–234. [PubMed: 488353]

Marston SB, Redwood CS. The essential role of tropomyosin in cooperative regulation of smooth muscle thin filament activity by caldesmon. J Biol Chem 1993;268:12317–12320. [PubMed: 8509369]

Mateos J, Herranz R, Domingo A, Sparrow J, Marco R. The structural role of high molecular weight tropomyosins in dipteran indirect flight muscle and the effect of phosphorylation. J Muscle Res Cell Motil 2006;27:189–201. [PubMed: 16752200]

Maytum R, Lehrer SS, Geeves MA. Cooperativity and switching within the three-state model of muscle regulation. Biochemistry 1999;38:1102–1110. [PubMed: 9894007]

Mazzei GJ, Kuo JF. Phosphorylation of skeletal-muscle troponin I and troponin T by phospholipid-sensitive Ca2+-dependent protein kinase and its inhibition by troponin C and tropomyosin. Biochem J 1984;218:361–369. [PubMed: 6712619]

McKillop DF, Geeves MA. Regulation of the interaction between actin and myosin subfragment 1: Evidence for three states of the thin filament. Biophys J 1993;65:693–701. [PubMed: 8218897]

McLachlan AD, Stewart M. Tropomyosin coiled-coil interactions: Evidence for an unstaggered structure. J Mol Biol 1975;98:293–304. [PubMed: 1195389]

McLachlan AD, Stewart M. The 14-fold periodicity in α-tropomyosin and the interaction with actin. J Mol Biol 1976;103:271–298. [PubMed: 950663]

Metzger JM. Myosin binding-induced cooperative activation of the thin filament in cardiac myocytes and skeletal muscle fibers. Biophys J 1995;68:1430–1442. [PubMed: 7787029]

Mirza M, Robinson P, Kremneva E, Copeland O, Nikolaeva O, Watkins H, Levitsky D, Redwood C, El-Mezgueldi M, Marston S. The effect of mutations in α-tropomyosin (E40K and E54K) that cause familial dilated cardiomyopathy on the regulatory mechanism of cardiac muscle thin filaments. J Biol Chem 2007;282:13487–13497. [PubMed: 17360712]

Moraczewska J, Hitchcock-DeGregori SE. Independent functions for the N- and C-termini in the overlap region of tropomyosin. Biochemistry 2000;39:6891–6897. [PubMed: 10841770]

Obenauer JC, Cantley LC, Yaffe MB. Scansite 2.0: Proteomewide prediction of cell signaling interactions using short sequence motifs. Nucleic Acids Res 2003;31:3635–3641. [PubMed: 12824383]

Palmiter KA, Kitada Y, Muthuchamy M, Wieczorek DF, Solaro RJ. Exchange of β- for α-tropomyosin in hearts of transgenic mice induces changes in thin filament response to Ca2+, strong cross-bridge binding, and protein phosphorylation. J Biol Chem 1996;271:11611–11614. [PubMed: 8662805]

Pardee JD, Spudich JA. Purification of muscle actin. Methods Enzymol 1982;85(Part B):164–181. [PubMed: 7121269]

Phillips GN Jr. Construction of an atomic model for tropomyosin and implications for interactions with actin. J Mol Biol 1986;192:128–131. [PubMed: 3820300]

Rao VS, La Bonte LR, Xu Y, Yang Z, French BA, Guilford WH. Alterations to myofibrillar protein function in nonischemic regions of the heart early after myocardial infarction. Am J Physiol Heart Circ Physiol 2007;293:H654–H659. [PubMed: 17400716]

Rasband, WS. NIH Image, ImageJ. Bethesda, Maryland: National Institutes of Health; 1997.

Regnier M, Rivera AJ, Wang CK, Bates MA, Chase PB, Gordon AM. Thin filament near-neighbour regulatory unit interactions affect rabbit skeletal muscle steady-state force-Ca(2+) relations. J Physiol 2002;540:485–497. [PubMed: 11956338]

Sano K, Maeda K, Oda T, Maeda Y. The effect of single residue substitutions of serine-283 on the strength of head-to-tail interaction and actin binding properties of rabbit skeletal muscle α-tropomyosin. J Biochem (Tokyo) 2000;127:1095–1102. [PubMed: 10833280]

Shiverick KT, Thomas LL, Alpert NR. Purification of cardiac myosin. Application to hypertrophied myocardium. Biochim Biophys Acta 1975;393:124–133. [PubMed: 124593]

Singh A, Hitchcock-DeGregori SE. Local destabilization of the tropomyosin coiled coil gives the molecular flexibility required for actin binding. Biochemistry 2003;42:14114–14121. [PubMed: 14640678]

Singh A, Hitchcock-DeGregori SE. Dual requirement for flexibility and specificity for binding of the coiled-coil tropomyosin to its target, actin. Structure 2006;14:43–50. [PubMed: 16407064]

Smillie LB. Preparation and identification of α- and β-tropomyosins. Methods Enzymol 1982;85(Part B): 234–241. [PubMed: 6289041]

Snook JH, Li J, Helmke BP, Guilford WH. Peroxynitrite inhibits myofibrillar protein function in an in vitro assay of motility. Free Radic Biol Med 2008;44:14–23. [PubMed: 18045543]

Sousa AD, Farah CS. Quantitative analysis of tropomyosin linear polymerization equilibrium as a function of ionic strength. J Biol Chem 2002;277:2081–2088. [PubMed: 11694540]

Svoboda K, Block SM. Biological applications of optical forces. Annu Rev Biophys Biomol Struct 1994;23:247–285. [PubMed: 7919782]

Swartz DR, Moss RL, Greaser ML. Calcium alone does not fully activate the thin filament for S1 binding to rigor myofibrils. Biophys J 1996;71:1891–1904. [PubMed: 8889164]

Toyoshima YY, Toyoshima C, Spudich JA. Bidirectional movement of actin filaments along tracks of myosin heads. Nature 1989;341:154–156. [PubMed: 2674720]

Uyeda TQ, Kron SJ, Spudich JA. Myosin step size. Estimation from slow sliding movement of actin over low densities of heavy meromyosin. J Mol Biol 1990;214:699–710. [PubMed: 2143785]

Vahebi S, Ota A, Li M, Warren CM, de Tombe PP, Wang Y, Solaro RJ. p38-MAPK induced dephosphorylation of α-tropomyosin is associated with depression of myocardial sarcomeric tension and ATPase activity. Circ Res 2007;100:408–415. [PubMed: 17234967]

VanBuren P, Work SS, Warshaw DM. Enhanced force generation by smooth muscle myosin in vitro. Proc Natl Acad Sci USA 1994;91:202–205. [PubMed: 8278365]

VanBuren P, Palmiter KA, Warshaw DM. Tropomyosin directly modulates actomyosin mechanical performance at the level of a single actin filament. Proc Natl Acad Sci USA 1999;96:12488–12493. [PubMed: 10535949]

Vibert P, Craig R, Lehman W. Steric-model for activation of muscle thin filaments. J Mol Biol 1997;266:8–14. [PubMed: 9054965]

Wu SC, Solaro RJ. Protein kinase C ζ. A novel regulator of both phosphorylation and de-phosphorylation of cardiac sarcomeric proteins. J Biol Chem 2007;282:30691–30698. [PubMed: 17724026]

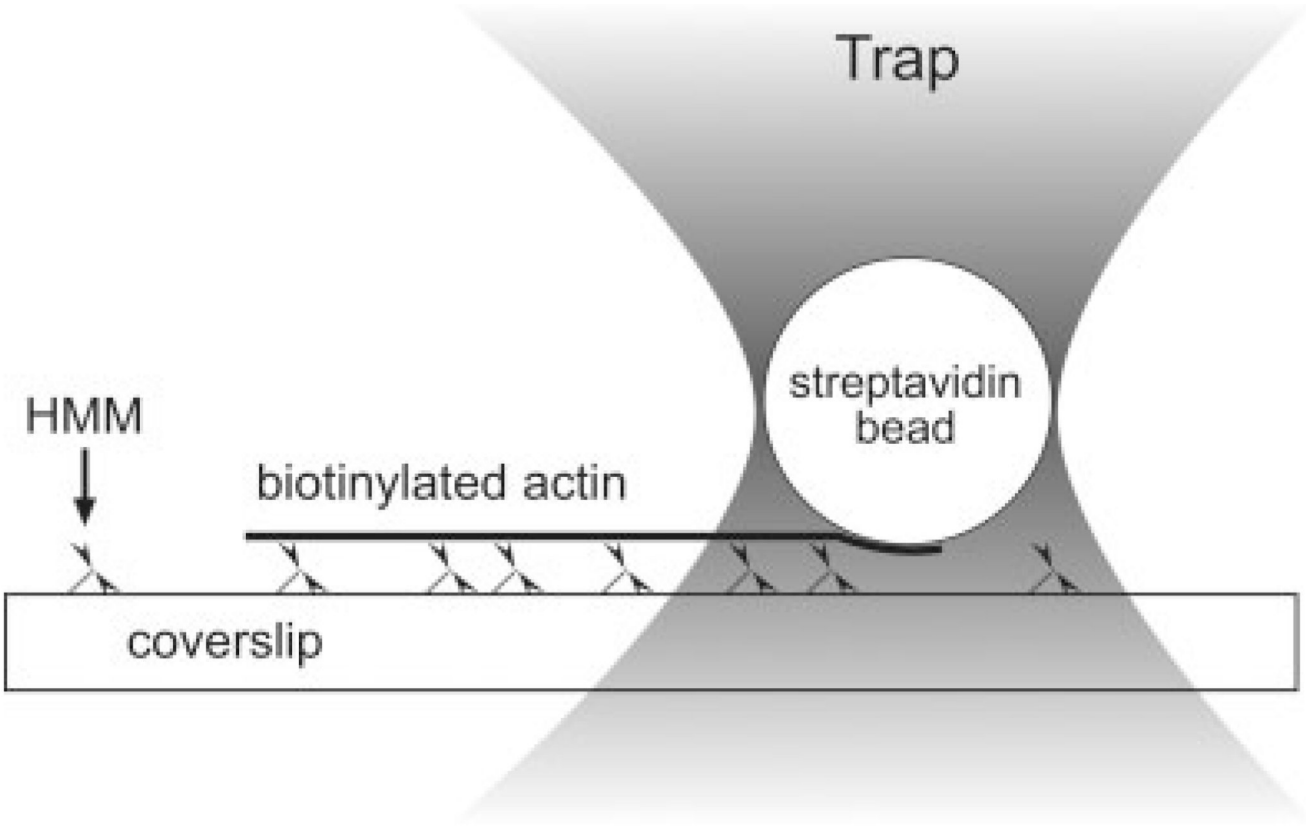

Fig. 1.

Schematic of the experimental set-up within a typical flow cell. HMM is adhered to a myosin coated surface. Fluorescently labeled, Tm-decorated biotinylated actin filaments are added along with fluorescently labeled, streptavidin-coated microspheres. When ATP is added, the HMM heads propel attached actin filaments. An optical trap is used to capture a streptavidin coated bead and bring it into contact with the trailing end of a moving filament. While the filament is stalled, the attached bead is displaced from the trap center and this displacement is used to calculate the stall force of the filament. Figure not to scale.

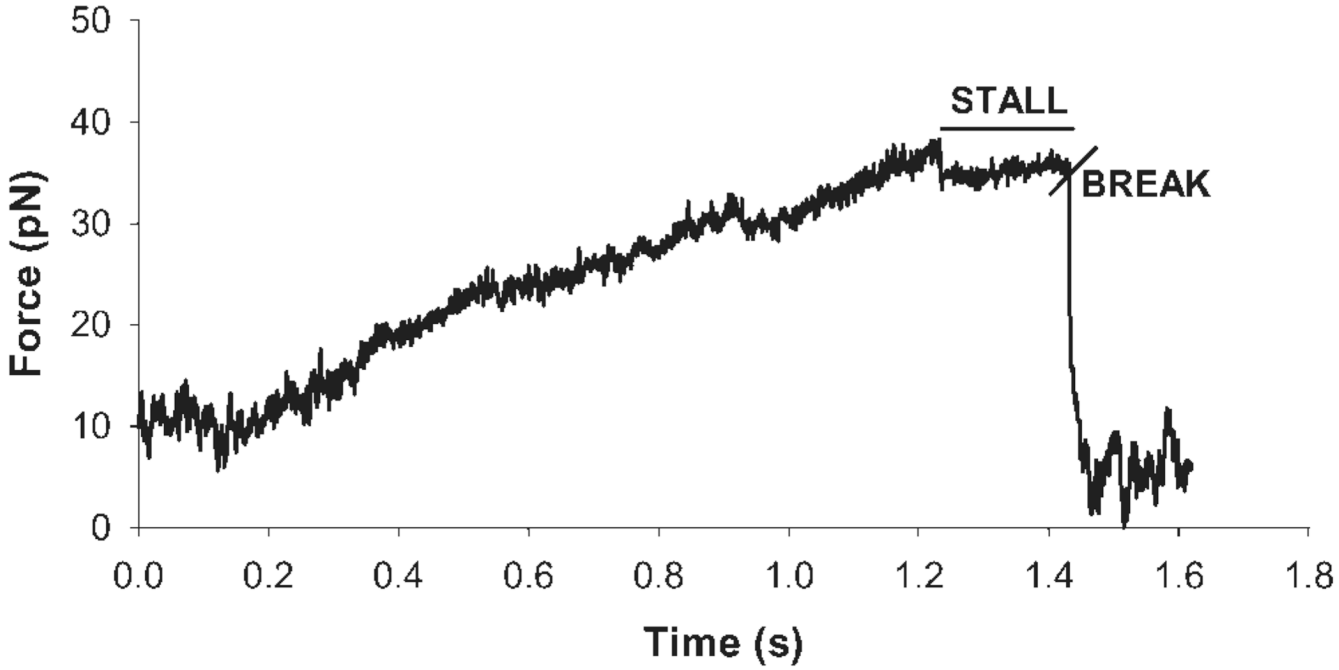

Fig. 2.

Typical stall force event. The trace remains at baseline until a trapped bead is brought into contact with a moving filament. As the filament moves while attached to the fluorescent streptavidin bead, there is a linear increase in force until the filament stalls. The rapid drop in force is illustrative of the filament detaching from the bead indicating the end of a stall force event.

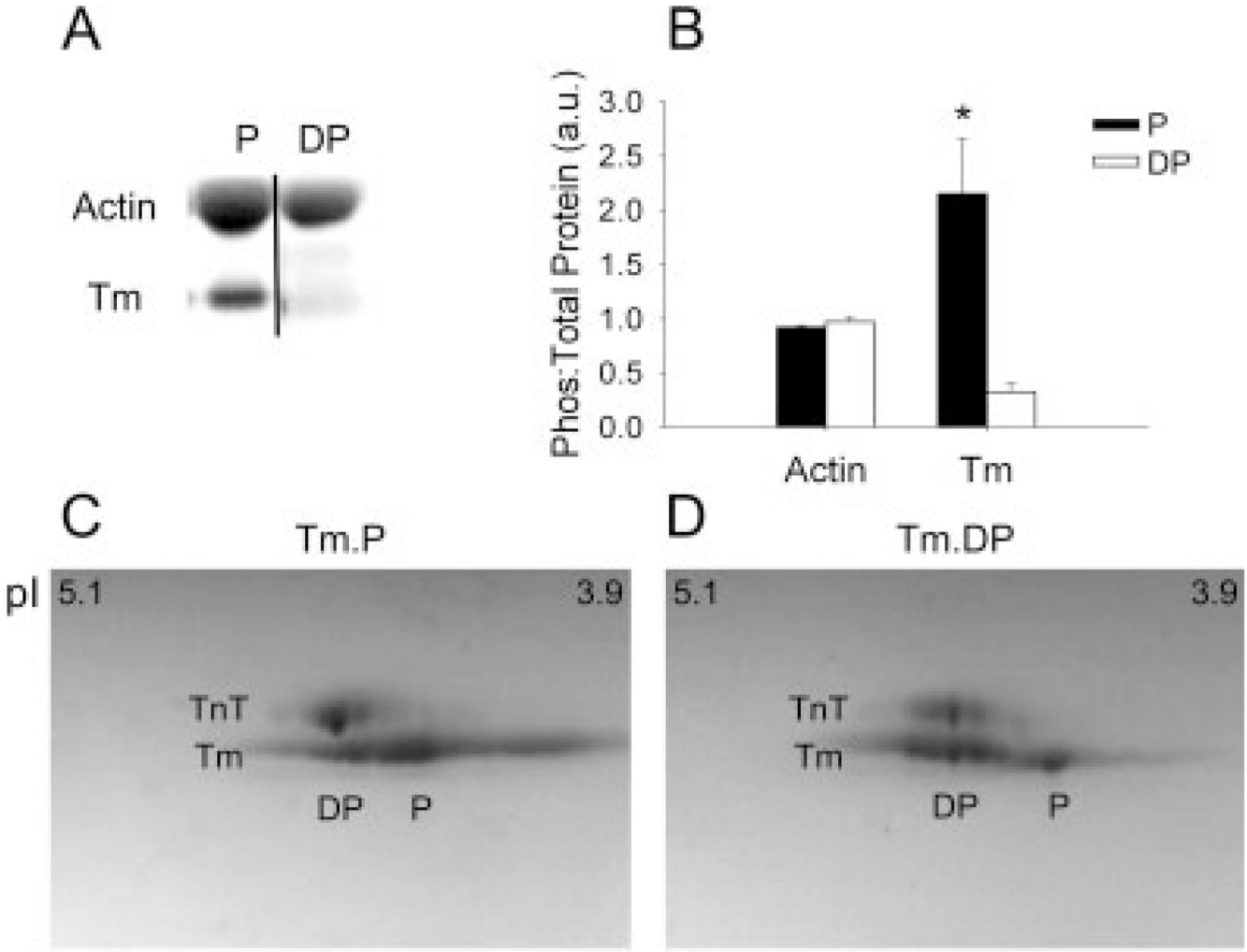

Fig. 3.

The results of phosphoprotein staining before and after dephosphorylation by alkaline phosphatase (AP). The gel image shows A+Tm.P (left) and A+Tm.DP (right). Actin stains non-specifically and shows no response to AP. Tm shows significant loss of phosphorylation after the addition of AP. The ratio of phosphorylation: total protein (Coomassie) is illustrated in the graph. Tm undergoes a significant decrease in phosphorylation following phosphatase treatment ($n = 3$), $P = 0.03$. (C) 2D PAGE of natively phosphorylated Tm (Tm.P). Phosphorylated (P) Tm shifts to a lower isoelectric point (pI). (D) 2D PAGE of dephosphorylated Tm (Tm.DP). Dephosphorylated (DP) Tm shifts to a higher pI. In both panels, troponin T (TnT) is present as it copurifies with Tm due to similar isoelectric points. However, TnT shows negligible phosphorylation.

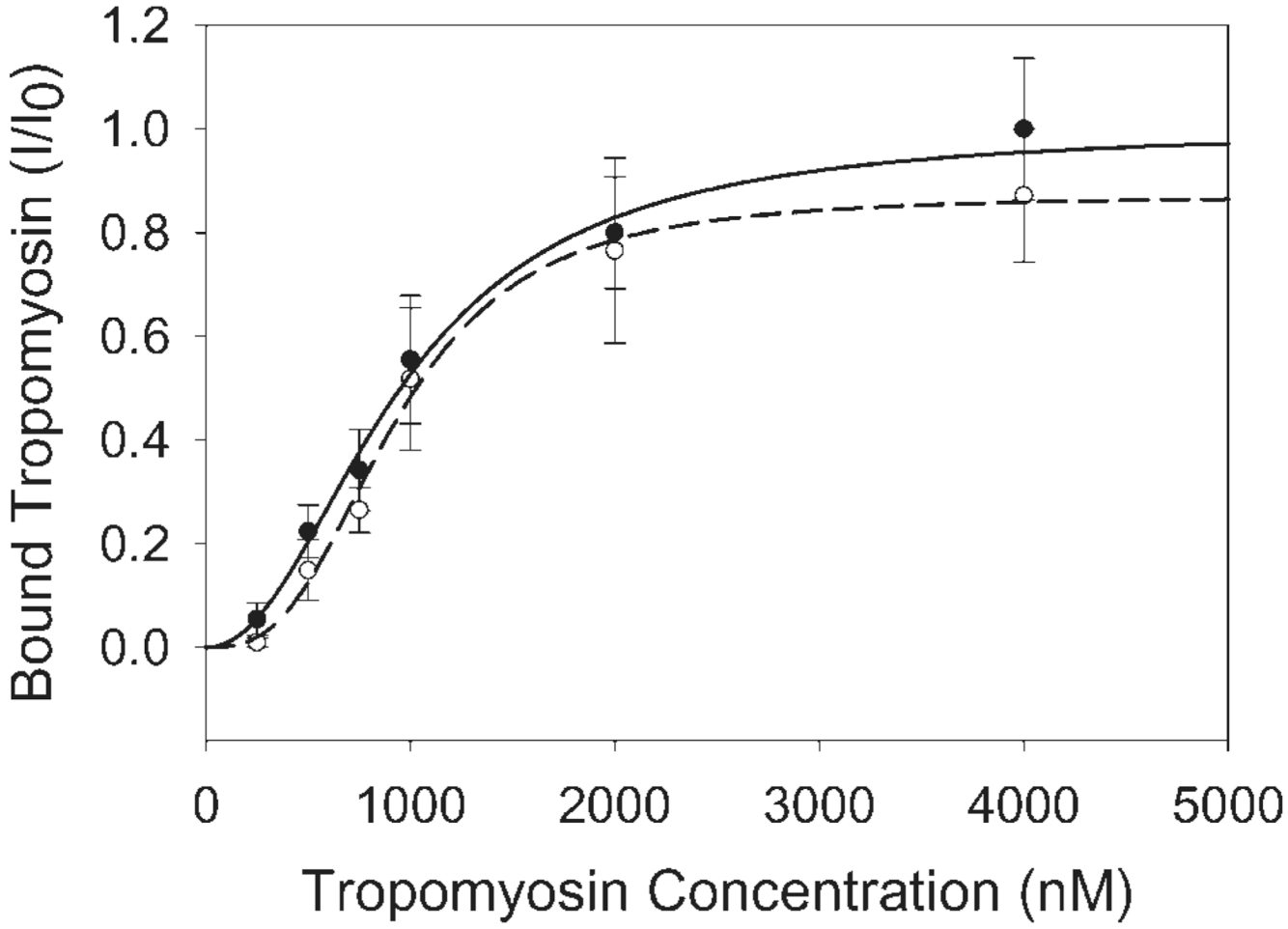

Fig. 4.

Actin-Tm Binding Curve. Bound Tm *versus* free Tm concentration was determined using 1 μM actin and cosedimentation. Actin-Tm binding was determined with both Tm.P (closed circles) and Tm.DP (open circles). A+Tm.P binding was not significantly different from A +Tm.DP binding. Both curves also illustrated cooperative binding. I is the electrophoretic band intensity of bound Tm, while I_0 is the bound Tm band density measured at 4 μM free Tm.P. All samples were normalized to I_0.

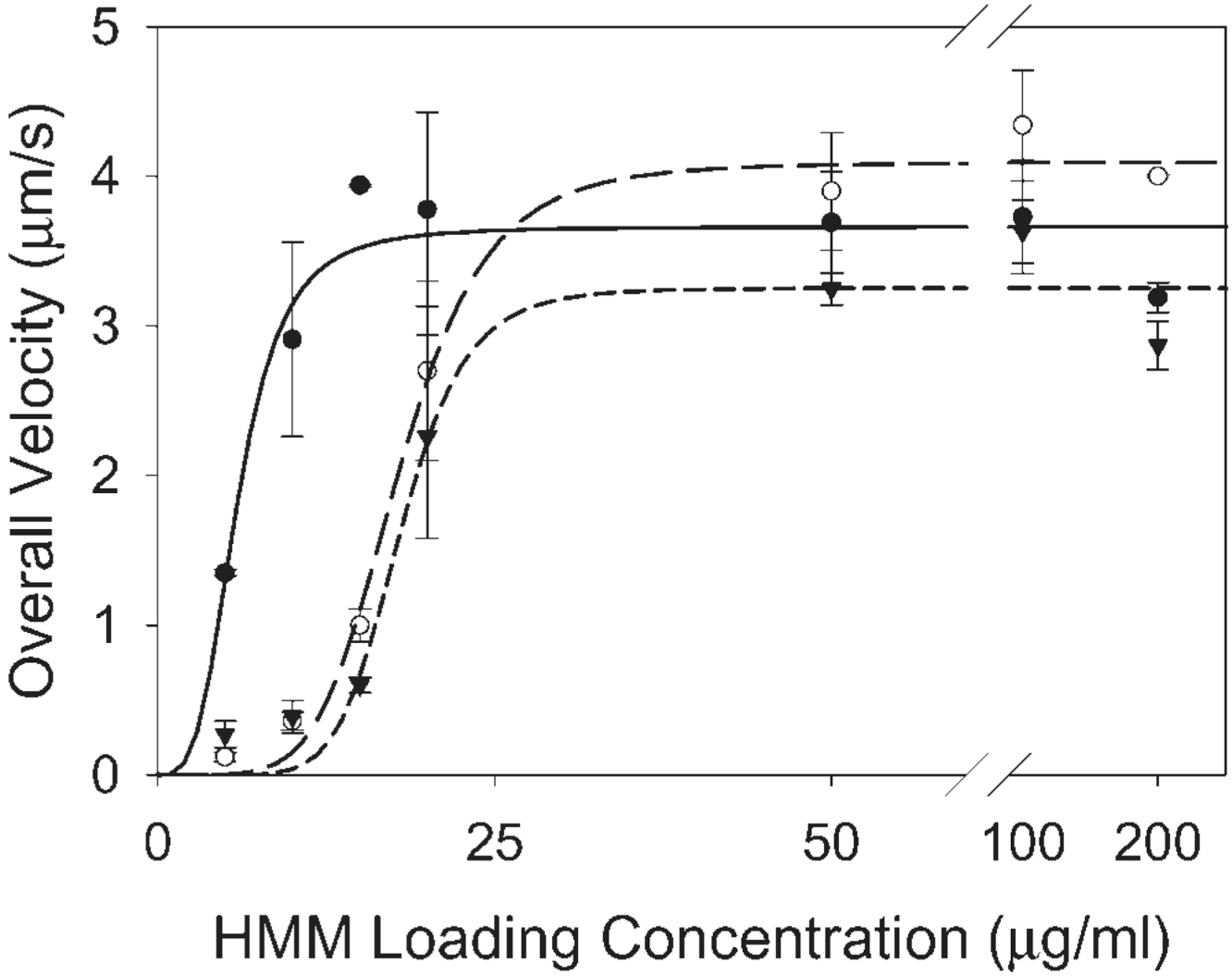

Fig. 5.

Effects of Tm phosphorylation states at a range of HMM head densities (5–200 µg/mL). Actin (closed circles) and A+Tm.DP (closed triangles) differed from A+Tm.P (open circles) at a saturating HMM head density (200 µg/mL). Hill fits revealed significant differences in the HMM concentrations for half-maximal velocity for actin (solid line) compared to A+Tm (long dashed line). P and A+Tm.DP (short dashed line).

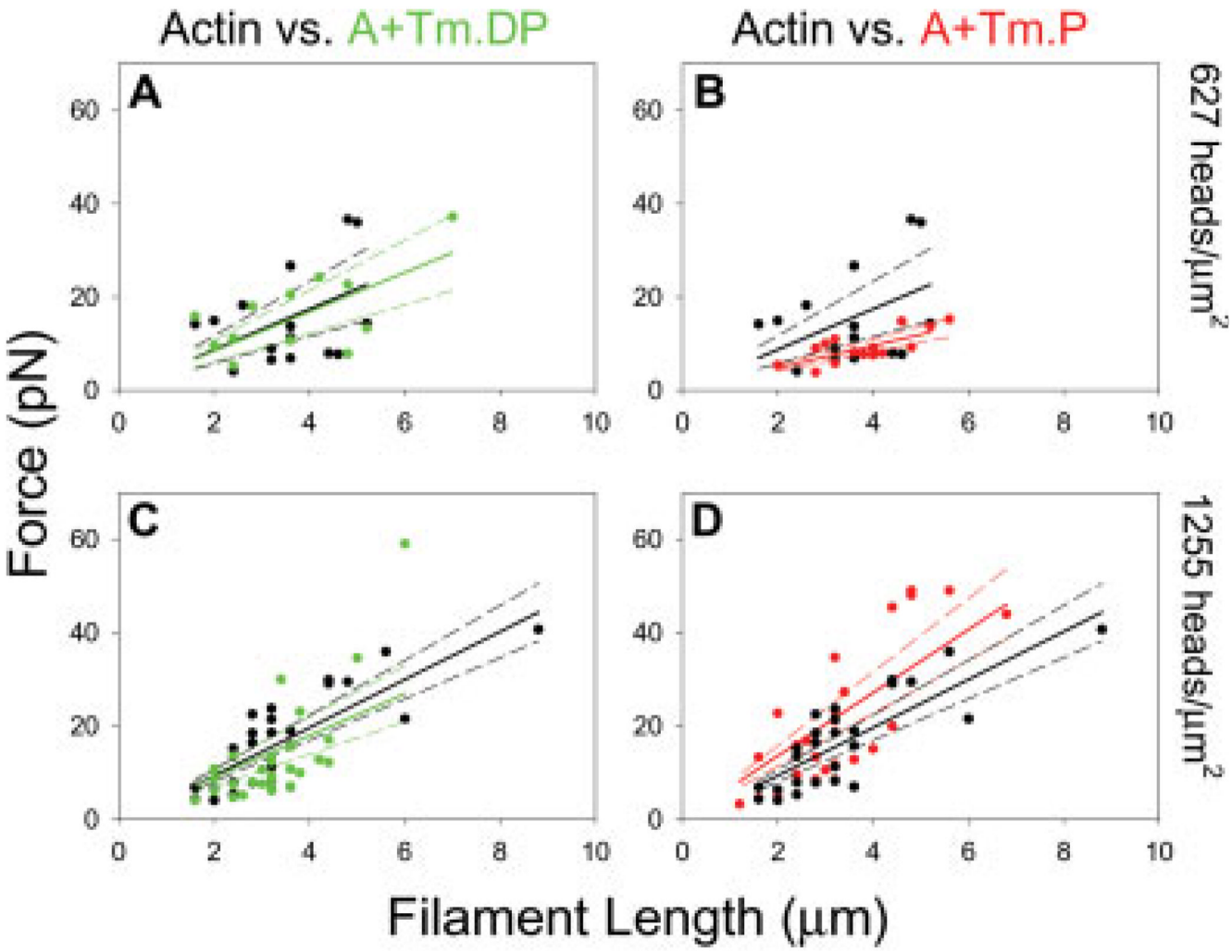

Fig. 6.

Force vs. filament length for representative conditions. Average isometric force measurements were obtained using optical trapping techniques over a range of filament lengths. Using linear regression the force/μm (solid lines) and 95% confidence intervals (dashed lines) of each experimental condition were determined. (A). Force vs. filament length measurements of actin (black) and A+Tm.DP (green) at low HMM head density. (B). Force vs. filament length measurements of actin and A+Tm.P (red) at low HMM head density. (C). Force vs. filament length of actin and A+Tm.DP at intermediate HMM head density. (D). Force vs. filament length of actin and A+Tm.P at intermediate HMM head density. Low HMM density = 627 heads/μm^2. Intermediate HMM density = 1255 heads/μm^2.

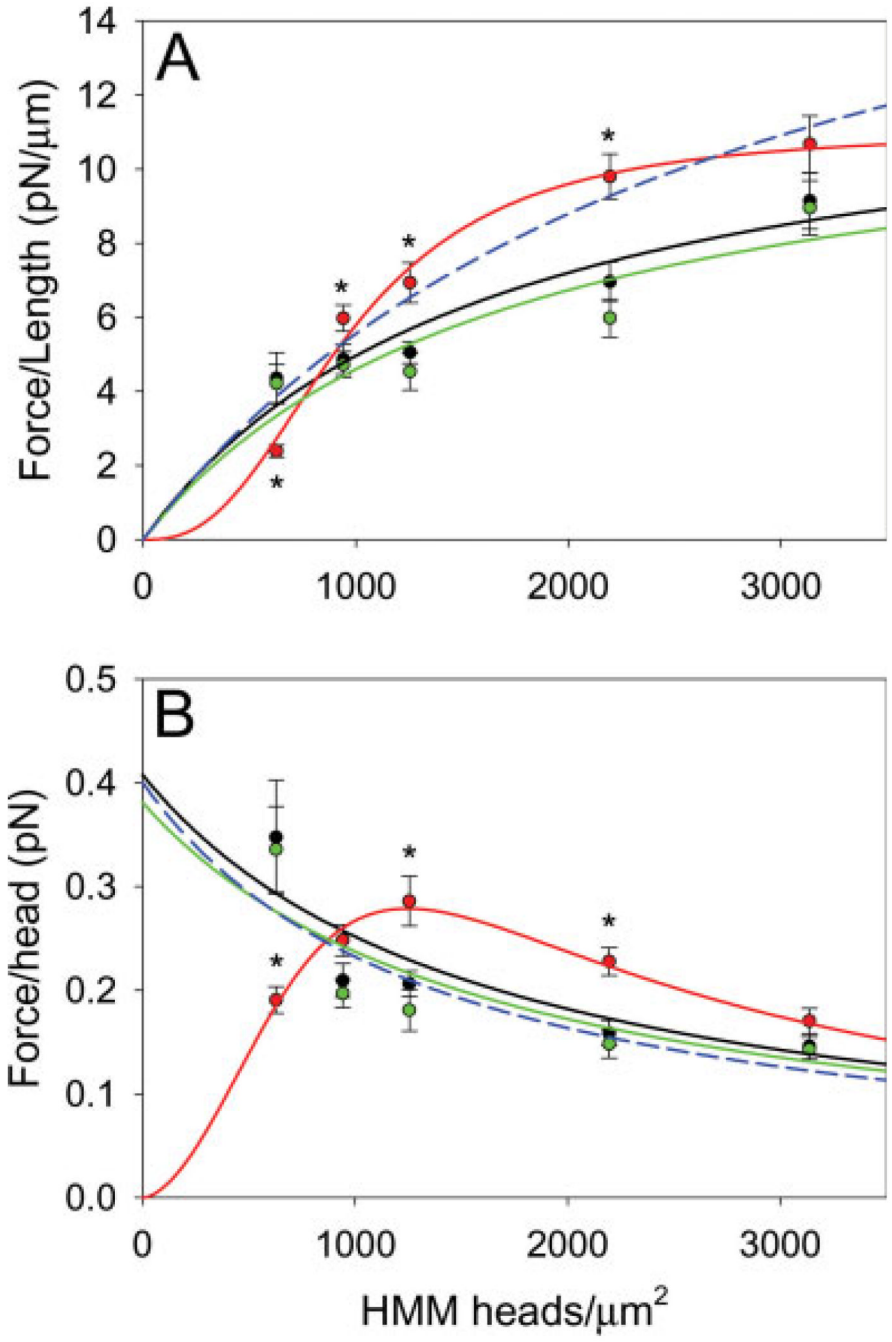

Fig. 7.

(A) f_{length} vs. Head Density. The force per filament length at the measured HMM surface densities was fitted using Eq. 1. Bare actin (black line) and A+Tm.DP (green line) behaved according to simple saturation kinetics. A+Tm.P (red line) exhibited cooperative behavior. A non-cooperative fit of A+Tm.P is also shown (blue dashed line). (B) f_{head} vs. Head Density. Force per head was also plotted as a function of HMM surface densities and fitted according to Eq. 3. Bare actin (black line) and A+Tm.DP (green line) showed a steady decline in force production with increased HMM density. However, A+Tm.P (red line) increased to a maximum force production at the intermediate HMM density. A non-cooperative fit of A

+Tm.P is also shown (blue dashed line). * indicates significance between A+Tm.P vs. bare actin and A+Tm.DP ($P < 0.05$).

TABLE I

The f_{length} Values at Each HMM Head Density and Corresponding Standard Errors

	f_{length} (pN/μm)[a]				
	10 μg/mL and 627 heads/μm^2	**15 μg/mL and 941 heads/μm^2**	**20 μg/mL and 1255 heads/μm^2**	**35 μg/mL and 2196 heads/μm^2**	**50 μg/mL and 3136 heads/μm^2**
Actin	4.4 ± 0.7	4.9 ± 0.4	5.1 ± 0.3	7.0 ± 0.5	9.1 ± 0.8
A+Tm.P	2.4 ± 0.2	6.0 ± 0.4	6.9 ± 0.5	9.8 ± 0.6	10.7 ± 0.8
A+Tm.DP	4.2 ± 0.5	4.7 ± 0.3	4.5 ± 0.5	6.0 ± 0.5	9.0 ± 0.7

Values were calculated using linear regression. HMM loading concentrations and their associated surface HMM head densities are also shown.

[a] The f_{length} values at each HMM loading concentration (μg/mL) and corresponding HMM head density (heads/μm^2).

Cell Motil Cytoskeleton. Author manuscript; available in PMC 2009 October 29.

TABLE II

The f_{head} Values at Each HMM Head Density and Corresponding Standard Errors

	f_{head} (pN/head)				
	627[a]	**941**	**1255**	**2196**	**3136**
Actin	0.35 ± 0.05	0.21 ± 0.02	0.21 ± 0.01	0.16 ± 0.01	0.15 ± 0.01
A+Tm.P	0.19 ± 0.01	0.25 ± 0.01	0.29 ± 0.02	0.23 ± 0.01	0.17 ± 0.01
A+Tm.DP	0.34 ± 0.04	0.20 ± 0.01	0.18 ± 0.02	0.15 ± 0.01	0.14 ± 0.01

Values were calculated using linear regression.

[a]The values 627, 941, 1255, 2196, and 3136 represent HMM head density (heads/μm2).